Coalescence kinetics and microstructure evolution of Cu nanoparticles sintering on substrates

a molecular dynamics study

Liu, Xu; Li, Shizhen; Tan, Chunjian; Gao, Chenshan; Liu, Yang; Ye, Huaiyu; Zhang, Guoqi

DOI
10.1016/j.jmrt.2022.01.052

Publication date
2022

Document Version
Final published version

Published in
Journal of Materials Research and Technology

Available online at www.sciencedirect.com

jmr&t Journal of Materials Research and Technology

journal homepage: www.elsevier.com/locate/jmrt

Original Article

Coalescence kinetics and microstructure evolution of Cu nanoparticles sintering on substrates: a molecular dynamics study

Xu Liu [a,b,1], *Shizhen Li* [b,1], *Chunjian Tan* [a,b], *Chenshan Gao* [b,c], *Yang Liu* [d], *Huaiyu Ye* [b,c,*], *Guoqi Zhang* [a]

[a] *Department of Microelectronics, Delft University of Technology, 2628 CD, Delft, the Netherlands*
[b] *School of Microelectronics, Southern University of Science and Technology, Shenzhen 518055, China*
[c] *The Key Laboratory of Optoelectronic Technology & Systems, College of Optoelectronic Engineering, Education Ministry of China, Chongqing University, Chongqing 400044, China*
[d] *School of Materials Science and Chemical Engineering, Harbin University of Science and Technology, Harbin, 150040, China*

ARTICLE INFO

Article history:
Received 1 November 2021
Accepted 9 January 2022
Available online 15 January 2022

Keywords:
Cu nanoparticle
Sintering on substrate
Microstructural analysis
Sintering dynamics
Molecular dynamics

ABSTRACT

Nano copper sintering technology has great potential to be widely applied in the wide-bandgap semiconductor packaging. In order to investigate the coalescence kinetics of copper nano particles for this application, a molecular dynamic (MD) simulation was carried out at low temperature on a special model containing two substrate and multiple particles in between. Accordingly, thorough microstructure and dislocation investigation was conducted to identify the atomic-scale evolution in the system. The corresponding findings could provide evidence on the new particle-substrate sintering mechanism. Furthermore, atomic trajectories tracking method was applied to study the rotation behavior of different sized nano particles. New rotation behavior and mechanism were described. Additionally, the study on the size effect of copper particles on the sintering process and coalescence mechanism was conducted via comparing the microstructural and dislocation distribution of 3 nm, 4 nm and 5 nm models. Finally, by comparing the MSD results at low and high temperature for each model, the dominant coalescence dynamics changes were obtained.

1. Introduction

Semiconductor technology is key to modern industrial system. For the past few years, wide-bandgap (WBG) semiconductors materials, such as SiC and GaN, are receiving extensive attention due to their excellent electrical, thermal and mechanical properties. For operating at higher operating temperature and higher power density, the interconnecting materials must also be improved to ensure the higher reliability requirement raised

* Corresponding author.
E-mail address: yehy@sustech.edu.cn (H. Ye).
[1] These authors contributed equally to this work.

https://doi.org/10.1016/j.jmrt.2022.01.052

by WBG semiconductor devices. Soldering and brazing are the techniques which create metallic joints without melting of the base material. However, conventional Pb-free soldering materials such as SnAgCu (SAC) alloys with reflow temperature of 220–260 °C exhibit poor reliability at high temperature. Alternative joining techniques such as nano-silver sintering [1–8] and transient liquid phase soldering (TLSP) method [9–11] have been reported, as they can withstand the high temperature caused by high power density. However, the largescale production of silver sintering material and TLPS material both are costly. In recent years, nano copper sintering technology is gaining more and more attention. Compared to silver, copper is much more cost-effective (about 1% of the price) and has sufficiently high conductivity and good resistance to ion migration [12–18].

Generally, sintering is a thermally activated process improving the material strength via particle necking connection and microstructural network formation. On a microscopic scale, such process occurs through atomic transportation (mass transportation) at the contact area of particles [19,20]. According to the research on the high temperature sintering, the dominant mass transportation mechanisms include 1) Evaporation and recondensation, 2) Surface diffusion, 3) Volume diffusion beneath the surface, 4) Grain boundary diffusion, 5) Volume Diffusion [19]. However, in the field of semiconductor packaging, the device usually can only withstand process temperature below 300°C [20], and as a result, most of above mentioned high-temperature mechanism cannot be activated.

In order to deeply understand the nano particles (NPs) coalescence mechanism at low temperature, atomic-scale simulation methods such as Molecular Dynamics (MD) can be applied, which can help us to observe the microstructural evolution, dislocation behavior and diffusion process during the sintering [20–25]. It is reported that at low temperature the dominant mechanisms can include grain boundary diffusion, matrix diffusion, surface diffusion, plastic deformation mechanism, etc. [21,26–28]. However, most of the current research is based on two-particles or three-particles models, which focus on the necking formation, crystal rearrangement. There are limitations: Firstly, conventional double-particles model usually uses NVT ensemble, which is hardly to eliminate the negative influence of pressure random fluctuation. Secondly, in fact in the real semiconductor packaging process, the nano copper particles need to be sintered between a chip with metallization layer and a substrate with metal finishes. The interaction between different components may significantly influence the process such as particle contact, neck formation, stress distribution, pores generation and closure.

To use MD method to study the sintering between chip and substrate is very challengeable. Hai Dong et al. [29] showed that metallic nanoparticles can be deposited on the substrate in 400 ps through necking formation. E. Elkoraychy [30] used a similar model to explore homogeneous sintering and heterogeneous sintering. It is found that due to the constraints effect by the substrate, the particles were twisted and formed grain boundaries in between. In the meantime, the particles penetrated into the substrate. Lan Zhan et al. [31] set particles on different sites and on a substrate with different orientations for sintering, and they found that the grain boundaries formed by the substrate and the particles during sintering could promote the generation of dislocations. Then the particles would rotate and move slightly to eliminate the grain boundaries. Jiaqi Wang [32] et al. conducted transient liquid phase sintering simulation of Ni nanoparticles on an alloy substrate and stated that Ni nanoparticles in the matrix have stronger diffusion properties. The all-above-mentioned studies are based on double-particles model or single-particle-substrate model. The interactions between different components at each stage and the corresponding coalescence kinetics have not been discussed yet. Dai Ishikawa et al. [33]used a model containing multi-particle with substrate for the first time, and they mainly explored the diffusion behavior between Cu nanoparticles and different metal finishes. Whereas, sintering mechanism, pores evolution has not been discussed. Overall, among the sintering model with multiple particles on substrates, there is still a lack of theory concerning the sintering behavior, microstructure evolution, and sintering mechanisms.

In present work, by using the MD simulation method, we set up a model system including two substrates and nine 4 nm Cu particles in between. The 500 K low-temperature sintering process of this structure was deeply studied and the microstructure change, crystalline evolution, the dislocation generation and annihilation were monitored by carrying out Common Neighbor Analysis (CNA), Dislocation Extraction Algorithm (DXA) analysis. Then the atomic diffusion activities were studied by analyzing the corresponding atomic mean-squared displacement (MSD) diagrams. In addition, the particle rotation phenomenon and pores evolution during the sintering process had been well studied. Finally, the size effect of Cu nano particles on the sintering process and mechanisms in this complex system were discussed.

2. Methods

In this study, all MD simulation works were conducted by using LAMMPS [34]. The embedded atom method [35] (EAM) potential developed by Fischer [36] was used to describe the low-temperature atomic interactions among copper atoms in particles and substrates. In this study, a special sandwiched-like model containing two substrate and multiple particles in between was applied as shown in Fig. 1. Previous studies have dealt with typical models which applied different amounts of NPs and substrate as shown in Table 1. It turns out that in order to study the interaction between substrate and NPs, effect of size and temperature on sintering kinetics, microstructure and pores evolution during sintering, the model of double substrates with multiple NPs is a reasonable selection.

Previous studies stated that only a diameter of NP within 2.8–6 nm is able to disclose the sintering kinetics [29,41,45,46]. Accordingly, as shown in Fig. 1 the first model consisted of nine Cu nano particles with a diameter of 4 nm in 3 × 3 array was built. Then for the study of particle size effect, 3 nm and 5 nm Cu NPs models were developed as well. For all models, two copper substrates were set above and below the particle array. It is worth noting that the upper substate is used to

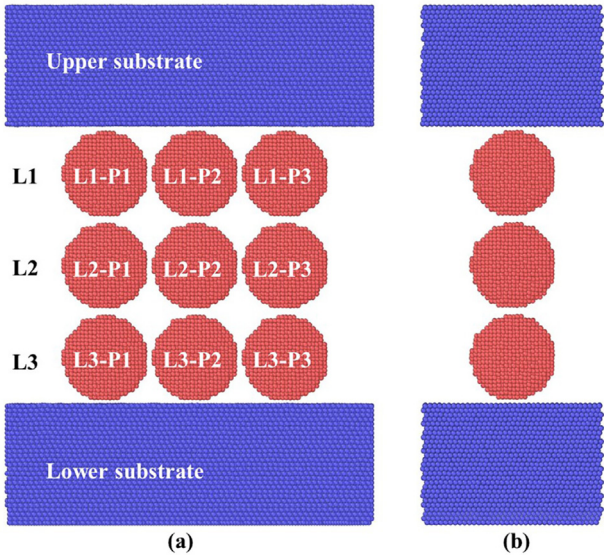

Fig. 1 – Initial configuration of the particle-substrate model for coalescence simulation. (a) Front view and (b) side view.

imitate the chip backside metallization layer in the packaging structure and the lower substrate represents the metallic finishes of power substrate. For description conveniency, the three layer of copper particles array are named as L1, L2 and L3 from top to bottom as shown in Fig. 1b. Within each layer, the particles are further labeled according to the order, for example, L1-P1, L1-P2 and L1-P3. Based on the previous study, the (111) plane is set as the plane exposed to the NPs in most cases due to its lowest surface energy [33]. In addition, the initial distance between NPs is usually within 2–5 Å [24]. Accordingly, in our study the spacing between particles is set as 3.61 Å. In order to avoid the particle spontaneous coalescence prior to the particle-substrate sintering, the upper and lower substrate had the (111) plane facing to the NPs with 3 Å initial gap between them.

Firstly, to obtain the equilibrated initial structure of constructed model, a relaxation step at 300 K for 500 ps in a NVT ensemble was conducted before the sintering process. Then for low temperature sintering study, a temperature profile with 1K/ps heating rate and 500 K peak temperature was applied to the system. The heating time was 200 ps. Finally, to study the size effect on coalescence kinetics the as-sintered system was then holding at 500 K for another 800 ps. We preset a small initial velocity (1 Å/ps, -z direction) to the atoms in the first two layers of upper substrate. The purpose of this setting is first to imitate the downwards movement tendency caused by the gravity of upper substrate (chip) and also to accelerate the simulation process. The effect of initial velocity value on the results was studied and could be found in the Supporting Information. In order to avoid the influence by the random fluctuation movement by the substrate, we fixed the coordinate of downmost two layers of lower substrate. In all simulations, periodic boundary conditions were applied in three dimensions. A timestep of 1 fs was set for data recording and the positions as well as velocities of each Cu atoms were recorded in every 1 ps.

OVITO was applied to visualize the atomic configurations and analyze the dislocation conditions. To describe the change on x-axial and z-axial, Shrinkage Ratio (SR, ζ_x) and Coalescence Index (CI, ζ_z) were applied. The SR for L1, L2, L3 and CI for the whole system are named as $\zeta_{x,L1}$, $\zeta_{x,L2}$, $\zeta_{x,L3}$, ζ_z respectively. The respective calculation equations are as following:

$$\zeta_x = \frac{\Delta L}{L_0} = \frac{L_0 - L_t}{L_0}$$

$$\zeta_z = \frac{\Delta H}{H_0} = \frac{H_0 - H_t}{H_0}$$

where L_0 and H_0 are the initial distance between particle in each layer and the initial distance between the upper and lower substrate. L_t and H_t are the corresponding distance at moment t. As previously mentioned, CNA and DXA analysis tools were used to analyze the crystal structures and dislocations evolution, respectively [47,48] Prior to using the method, the cutoff radius (r_{cut}) needed to be set, which is always as below for face-centered cubic (FCC) structure:

$$r_{cut}^{fcc} = \frac{1}{2}\left(\sqrt{1/2}+1\right)a_{fcc} \approx 0.854 a_{fcc}$$

where, a_{fcc} is the lattice constant of the corresponding atom in FCC structure. In this simulation, the cutoff radius of Cu is 3.08. The contribution of atomic diffusion on coalescence mechanism was estimated by analyzing the MSD of the system [49,50]. The definition equation is as following:

$$\langle d^2 \rangle = \{[r(t_0+\tau) - r_{com}(t_0+\tau)] - [r(t_0) - r_{com}(t_0)]\}^2$$

where t_0 is the initial time, τ is the observation moment, $r(t_0)$ is the coordinates of the atom at time t_0, and $r_{com}(t_0)$ is the centroid coordinates of the particle. $r(t_0+\tau)$ is the atomic coordinates of the atom at time τ, and $r_{com}(t_0+\tau)$ is the particle centroid coordinates of the atom at time τ. <> is the ensemble average computing operator.

3. Results and discussion

3.1. *Coalescence kinetics of NPs-Substrate model at low temperature*

Since the morphology of the sintered structure was stabilized after 200 ps, in this study, we mainly focus on the evolution of microstructure during within the first 200 ps during the phase II. As mentioned in previous section, OVITO was applied to conduct an in-depth microstructural analysis. CNA and DXA analysis tools were employed to analyze the crystal structures and dislocations evolution, respectively. In the atomic configuration figure, we assign different colors to the Cu atoms of particles and substrate, so as to facilitate the observation of different behaviors of particles, substrates and interface. The dark green, light green and grey circles represented face-centered cubic (FCC), close-packed hexagonal (HCP) and amorphous atoms in nano particles. The orange, yellow and dark grey circles were used to indicate FCC, HCP and amorphous atoms in substrates. In the DXA analysis results graph, the green and red dots were used to designate FCC

Table 1 – Summary of simulation models on study of NPs coalescence.

Nr. of substrate	Nr. of NPs	Model	Previous research topic and Ref.	Topic of present study that was not mentioned in previous works
None	Double		Study of the general sintering behavior and mechanism between two or more NPs [37–41], Effects of specific structures on the coalescence process [39–41]	• Contribution of substrate on the sintering process
None	Multiple	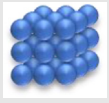		
Single	Single		Study of the interaction between single NP with substrate, misorientation effects, sintering of nanoflake (small)-NP, wetting and diffusion behavior [31,42,43]	• Additional interaction between different NPs and substrates simultaneously
Single	Multiple		Study of coalescence behaviors of NPs-substrate system and the homo- or heterogeneous effects [29,30,44]	• Effects of NPs and substrate from different direction.
Double	Single		Study of transient liquid phase sintering [32]	• Additional interaction between multiple NPs and substrates simultaneously. • Observation on the evolution of different type of pores.
Double	Double		Sintering process with the assisted-pressure and Stress-dislocation interaction during compression [24,45]	• More study on size and temperature effect. • Observation on the evolution of different type of pores.
Double	Multiple		The diffusion between NP and substrate [33]	• More study on size and temperature effect. • Observation on the evolution of different type of pores.

Table 2 – The maximum rotation angle for each model.

	3 nm	4 nm	5 nm
NP1-1	7°	3°	−3°
NP1-3	20°	6°	3°

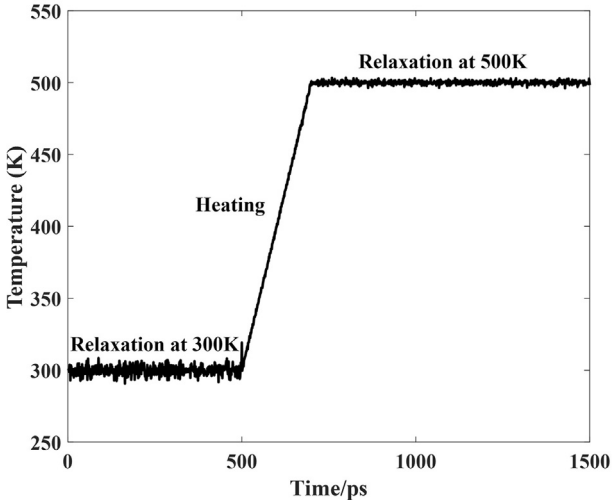

Fig. 2 – Temperature profile of sintering process at 500 K. Phase I is for relaxation. Phase II is for sintering process. Phase III is post-sintering process holding at peak temperature for another 800 ps.

atoms and HCP atoms, respectively. Green, yellow and blue lines represented Shockley dislocation, Hirth dislocation and perfect dislocation respectively.

Based on the simulation results, the whole sintering process can be divided into four stages for 4 nm model, which are: Stage I (0–40 ps, sintering of L1, L3 particles on corresponding substrates), Stage II (40–120 ps, sintering between L1 and L2 particles), Stage III (120–200 ps, sintering between L2 and L3 particles), Stage IV (after 200 ps, stabilization and recovery).

3.1.1. *Stage I*

As shown in Fig. 3(a)–(h), the atomic configurations among L1, L3 particles during Stage I are shown. In this stage, the upper substrate had downward motion with initial velocity of 0.067 Å/ps. Starting from 2ps, since the spacing between the substrate and the particle was smaller, the particle and substrate atoms sintering occurred first. As is observed from Fig. 3(a), necks formed first and grew fast on the interface of substrate and particles in both L1 and L3. The neck size was around 2.1 nm in L3 and 2.6 nm in L1. Then, Fig. 4 shows that there was slight increase of HCP content during this time, which was supposed to be from L1 and L3 as shown in Fig. 3(b) and (f). It is deduced that when NPs contact with substrate, the compress stress will first cause plastic deformation by generating stacking fault with small partial dislocation near the necking region. Apparently, the neck of L1 consisted of more of SF than that of L3 at this period, because the motion of upper substrate caused higher compressive force to the L1. Thus, higher driving force was provided through more plastic flow in L1. Small amounts of amorphous atoms were produced as well due to the crystal mismatch between particles and substrate surface.

Then till 10 ps, the sintering between substrates and L1, L3 were proceeding over time and the necking size increased to 3.18 nm and 3.64 nm for L3 and L1 respectively. In the meantime, the particles within L1 and L3 layer got interparticle contact with each other and began to form small necks. The interparticle neck size for L1 and L3 are only 0.76 nm and 1.35 nm at this moment. From Fig. 4a, the biggest shrinkage occurred at around this time period. According to the sharpest ramping peaks in both Fig. 4(b) and (c) of crystal fraction and dislocation, it indicates that a tremendous number of FCC atoms began to transform into amorphous and HCP. From the microstructural figure, we found that the SF grew rapidly and partial dislocation elongated a lot in both layers so far. This represents that severe plastic deformation occurred in these regions. These results suggest that the plastic flow was supposed to be the dominant coalescence mechanism at this stage. Interestingly, MSD results in Fig. 4d shows two extremely large slopes within this time span, which seems to imply drastic surface diffusion of particles. However, according to the study by Chen, this abnormal large slope indicates a much faster speed of atoms motion than what surface diffusion can allow, and thus the surface diffusion cannot play lead role in this period.

Finally, from 10 ps to 40 ps, both the interparticle sintering and substrate-particle sintering went forward and the neck size grew to almost the maximum size. In L1, the sintering proceeded more thorough than that in L3. There is still a large slope in MSD curve till 25 ps representing plastic-deformation induced atomic motion and then continued with a gentle slope representing surface diffusion. The atomic diffusion took in to effect at the final moment of this stage and in L3 the diffusion became dominant early than that of L1 as shown in Fig. 4d. Another evidence is that, the crystal structure evolution wears off during this period as shown in Fig. 4b. Instead, the SF with partial dislocation which generated at the early stage were eliminated through gliding, forming grain boundaries on the substate-particle interface. Consequently, it left many of particles free-of-defects as well as twining structure (in L1-P3). Since the formation of a stable stair-rod dislocation further decelerated the plastic flow of L3, it resulted in slower necking growth. In addition, small pores (Type I pore) formed around the particle-substrate necking region. As can be found in Fig. 4(c) and (d), the necking groove contained symmetrical curvature at the beginning (Fig. 4c). However, most of atoms moved to the side where the pores were used to be (Fig. 4d). Accordingly, it is believed that, the diffusion in the final moment was driven by the removing of free surface in these pores. At the end of this stage, the reduction of free surface caused by necking growth of L1 and L3 particles reached a brick wall. As a result, the particle Ex started to vibrate more or less periodically. It is worth noting that although at the beginning there was no misorientation among particles in L1 or L3, due to the pinning effect by substrates, the particles must conduct rigid rotation as a supplementary mechanism for the crystalline alignment. The details about rotation behavior would be discussed in the next section.

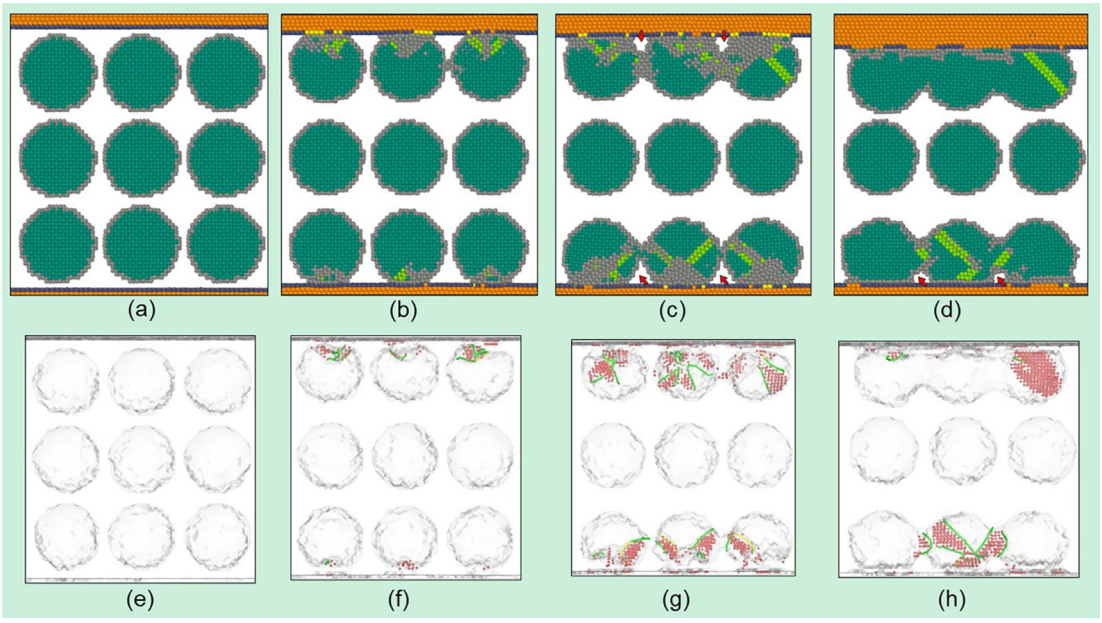

Fig. 3 – Cross-section and dislocation distribution snapshots of 4 nm model in Stage I. (a)–(d) Cross-section snapshots at 0 ps, 2 ps, 10 ps and 40 ps. (e)–(h) HCP and dislocation distribution snapshots at 0 ps, 2 ps, 10 ps and 40 ps. Type I pores were marked with red arrows.

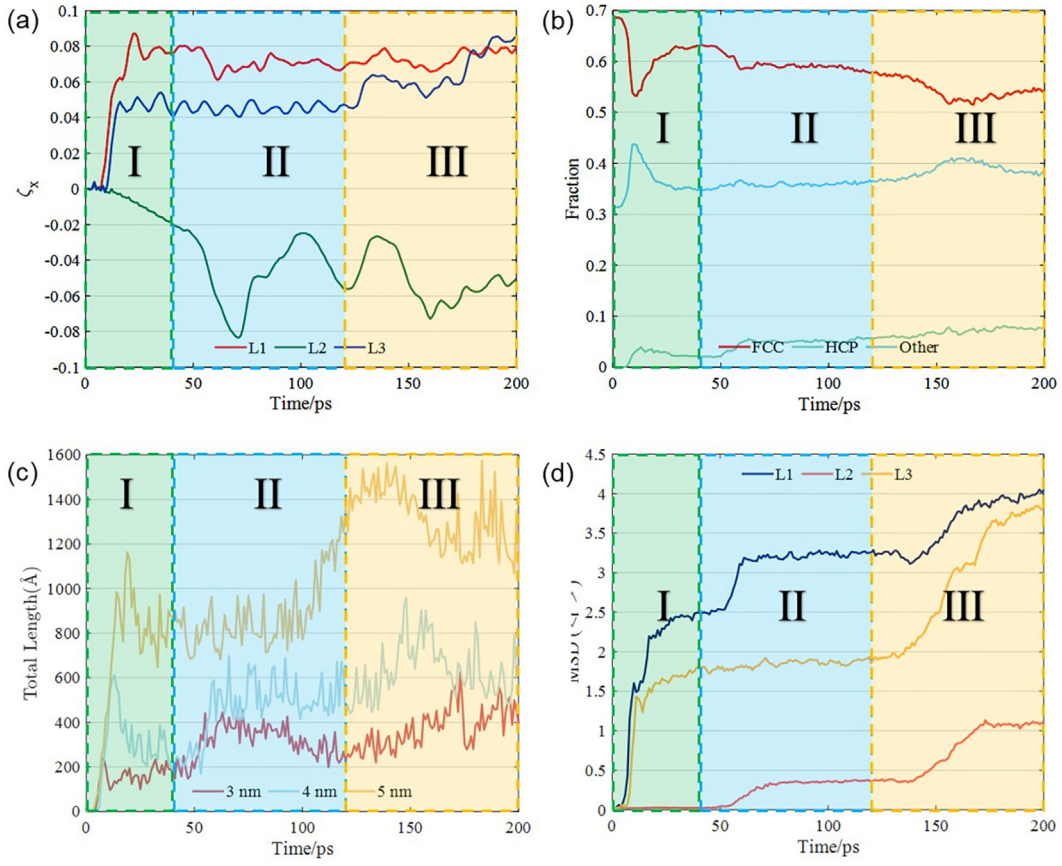

Fig. 4 – Macro- and microstructural evolution during 200 ps sintering. (a) The shrinkage of L1, L2 and L3. (b) The FCC, HCP and amorphous fraction. (c) The dislocation density. (d) The MSD curves for L1, L2 and L3.

3.1.2. *Stage II*

At Stage II (Fig. 5), the major process consisted of the sintering between L1 and L2, the interparticle sintering within L2. The interlayer shrinkage within L1 and L3 is almost finished. By analyzing MSD curve of L3, it is found that there was marginal diffusion occurring at this stage. In addition, due to the stair-rod dislocation in L3-P2, it also had high resistance to deform as shown in the atomic configuration and dislocation diagram. Small amount of plastic deformation by SF formation in L3-P3 and partial dislocation gliding on L3-P1 and L3-P2 interface. Therefore, for L3, the size of neck and pores did not change much at this stage. On the other side, the collision between particles in L1 and L2 caused interparticle stress on the interface. The stress was supposed to be larger than the critical resolved shear stress (CRSS) of the particles, and thus proceeded the gliding of partial dislocations in these particles and on their interfaces. Again, some amount of FCC transformed into HCP on dense packing plane and became amorphous atoms on the interface. Dislocation density raise again accompanied by the formation of SF. As is mentioned in previous content, the L1 particles would have rigid rotation for crystal alignment at Stage I. Consequently, particles in L2 would also rotate themselves by dislocation gliding and even slip across the grain boundary when contact with L1 [22,28,51]. Hence, the necks between L1 and L2 particles were likely to form at the lateral sites on L1 particles. Additionally, there was elastic stress on L1-P2 causing residual elastic oscillations (as shown in Fig. 2a) towards left and right [52]. Both of these two effects would further influence the interparticle coalescence in L2 randomly, because when two particles had great chance to sintering together, the other one would be isolated. For instance, in this work, the L2-P1 was the isolated one, whereas the L2-P2 and L2-P3 coalesced and forming the sintering networking. After the formation of such four-particles network, their further rotation was hindered and hence the misorientation within the network will exist for long time along with the existing of high-energy grain boundaries. In the middle of the network, a large pore formed which was referred to as Type II pore. From MSD curve for three layers at this stage, they all contained plateau till the end of this stage indicating the negligible diffusion behavior. Thus, the type I pores and type II pores cannot be vanished soon.

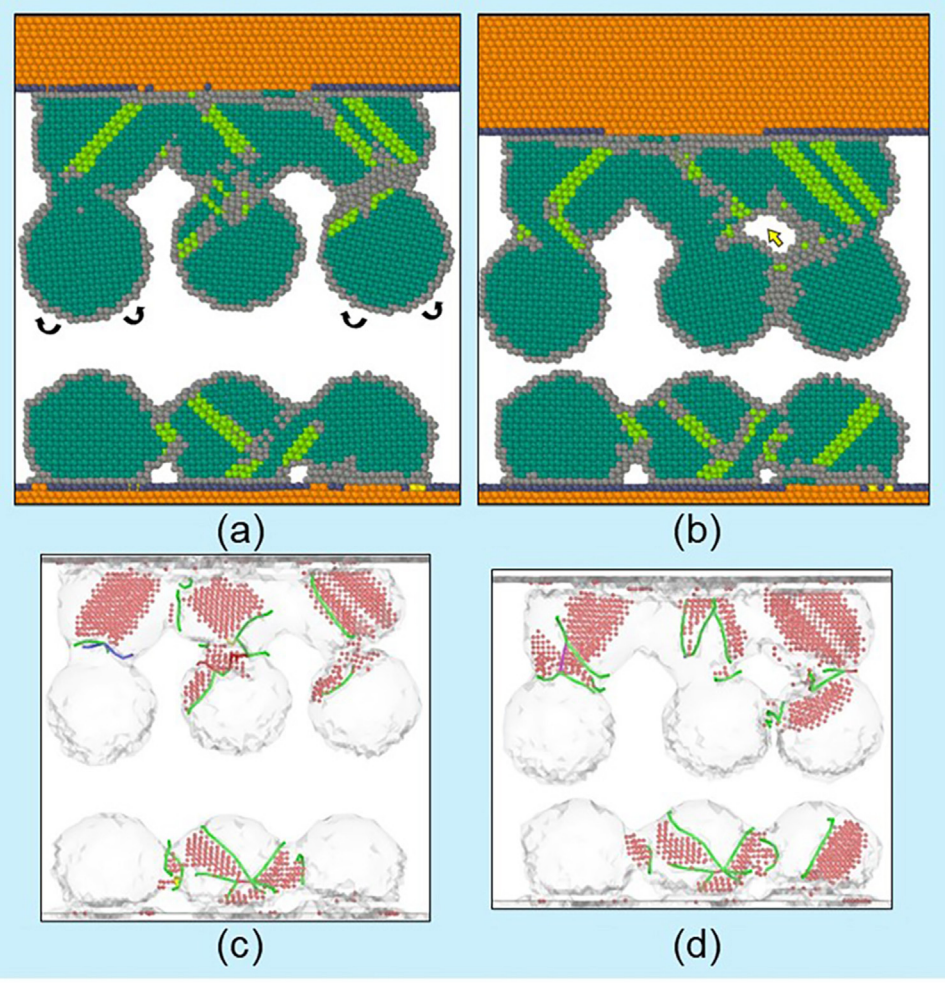

Fig. 5 – Cross-section and dislocation distribution snapshots of 4 nm model in Stage II. (a)–(b) Cross-section snapshots at 60 ps and 120 ps. (c)–(d) HCP and dislocation distribution snapshots at 60 ps and 120 ps. Type II pores were marked with yellow arrows.

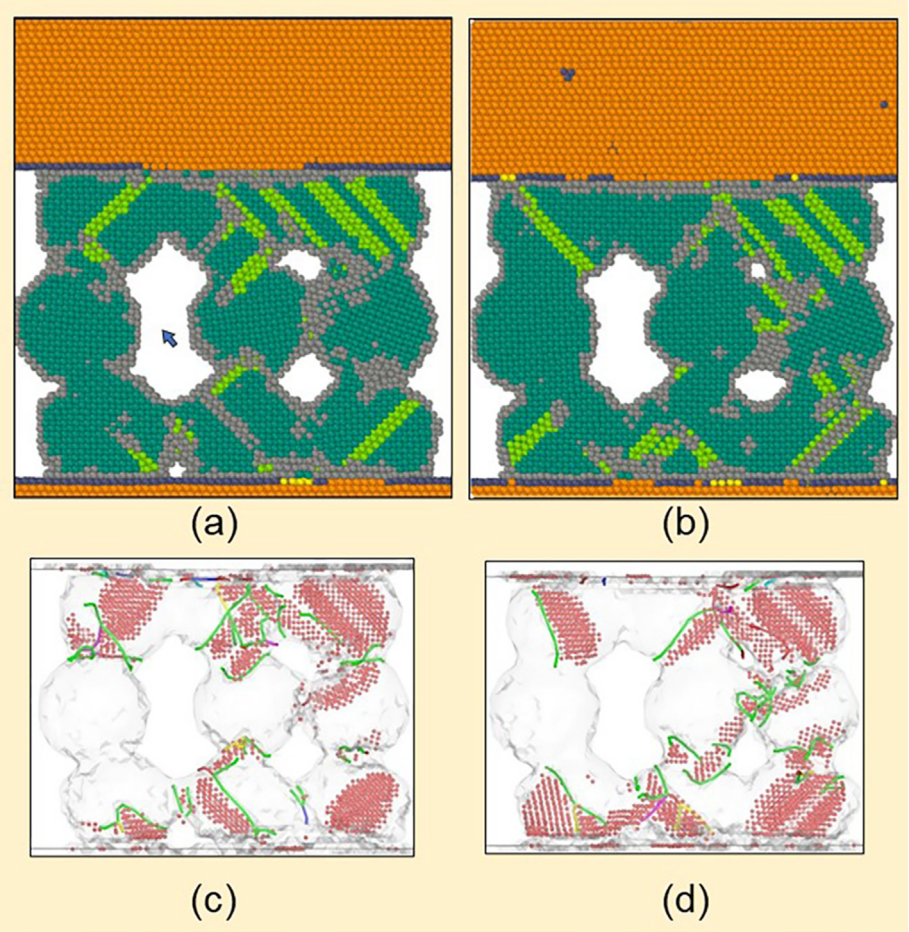

Fig. 6 – Cross-section and dislocation distribution snapshots of 4 nm model in Stage III. (a)–(b) Cross-section snapshots at 150 ps and 200 ps. (c)–(d) HCP and dislocation distribution snapshots at 150 ps and 200 ps.

3.1.3. *Stage III*

At the last stage (Fig. 6), L3 was compressed by the L2 particles and the coalescence within the model was further propelled. Under the great pressure given by substrate-L1-L2 system to L3 layer, lots of SF and dislocation were produced in L3-particles and necking region. At 150 ps, the huge compressive stress caused dissociation of stair-rod dislocation. Along with the dissociation of dislocation, extension of SF, the neck size between L2-particles and L3-particles grew fast. Most of dislocations glided to the interfaces between particles forming grain boundaries. After that, till 200 ps, the plastic flow almost finished with the decrease of dislocation density and HCP amount. As plotted in Fig. 2d, it is believed that the surface diffusion played more important role in this stage than at the beginning. The driving force was supposed to be the pores vanishing. The huge pores between L1 and L2 was becoming

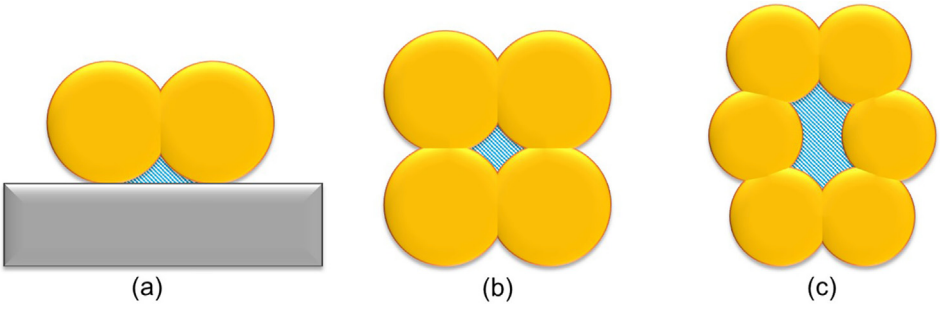

Fig. 7 – The schematic diagram of the three types of the pore. (a) Type I pore marked with blue grid was surrounded by a substrate and double particles. (b) Pore 2 was surrounded by four particles. (c) Pore 3 was generated by misorientation of between NPs.

smaller, and the MSD curve is increasing continuously even after 200 ps. With the vanishing of type I pores in L1, the MSD curve came to a plateau.

In summary, by analyzing the sintering process of this substrate-multi-particle model, we found that: 1) In this model, the dominating sintering mechanism at low temperature was plastic flow caused by dislocation production and motion. 2) The pressure provided by the upper substrate can significantly accelerating the sintering behavior by amplifying the plastic flow. 3) The rigid rotation might cause random misorientation and elastic oscillation of particles. 4) The pinning effect of substrate on particles might expand such random motion of particles in L2, which would produce huge pores. 4) Pores can be vanished via both plastic deformation and surface diffusion.

3.2. *Pores evolution and rotation behavior of NPs-Substrate model in low-temperature sintering process*

Generally, there were three types of pores in this system, as shown in Fig. 7. Type I was generated between as-connected NPs and substrate surface. Normally the pores can be closed through atomic diffusion [26]. The driving force is the extra free surface energy caused by the necking region. However, at low temperature, the diffusion is relatively slow, and hence the type I pores could not be filled soon via this way. In fact, due to the pressure induced by upper substrate, the plastic deformation of L1 caused by SF and dislocation movement could assist this process. This effect worked also for Type II pores. When four particles were contacting with each other, a small pore will be formed in the middle of such sintering network. This type of pores was always with small size and could be filled fast via plastic flow of all four particles. The last type of pore was formed because of the misorientation for particles in L2 with particles in L1 and L3. For crystal alignment, the L2 particles would rotate with small angles after forming neck with L1 particle, which might cause big gap between L2 particles. Since the pore III size is too big, both the surface diffusion and plastic flow cannot work.

For the rotation behavior, it is reported in the literature that the rigid rotation of particles during low-temperature sintering could be divided into two categories: 1) When there is an initial misorientation between particles, the particle alignment process will appear via dislocation gliding through adjacent particles. The driving force was attributed to surface stress in the neck groove and as a result, it would remove or reduce the particles interface associated with grain boundaries and cause the reduction of total system energy [52,53]. 2) when there is no misorientation between crystal, the rotation can occur as well. It is reported that, small particles could have a fast crystallization process when their connected faces are perfectly matched. And then due to the driving force of annihilation of free surfaces, the crystallized structure at neck region would become amorphous again to reduce the

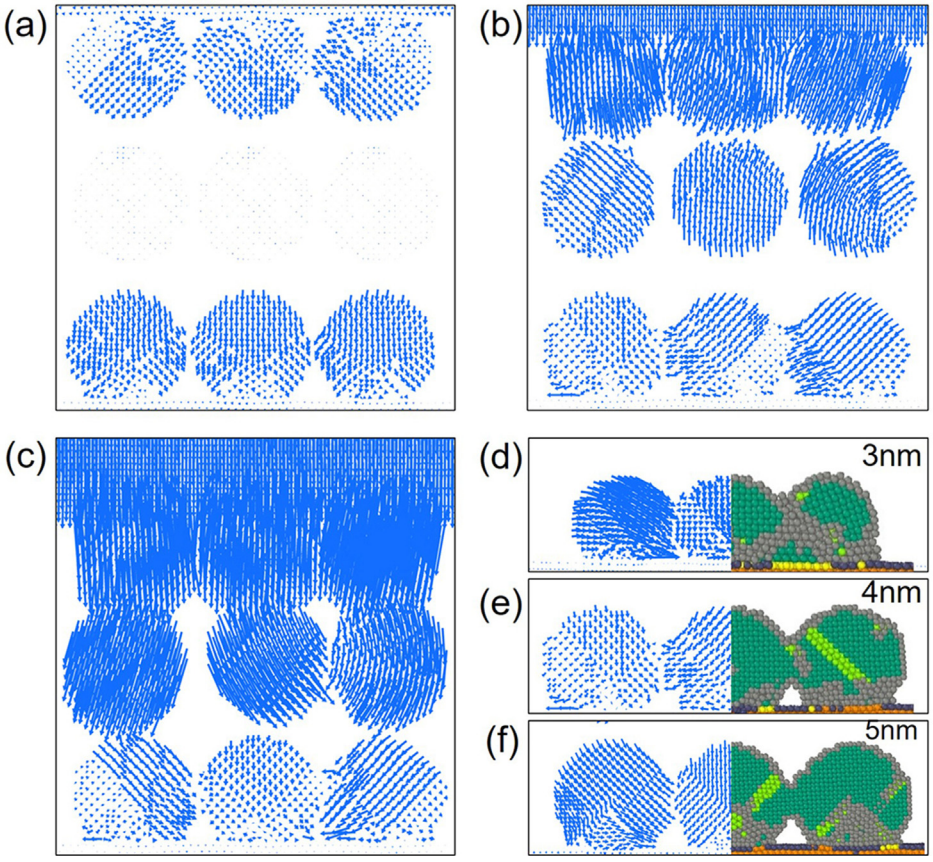

Fig. 8 – Displacement vectors of the atoms of the 4 nm model at 500 K. (a) at 10 ps. (b) at 60 ps. (c) 120 ps. Displacement vectors of L3 atoms at 60 ps of the (d) 3 nm model, (e) 4 nm model and (f) 5 nm model.

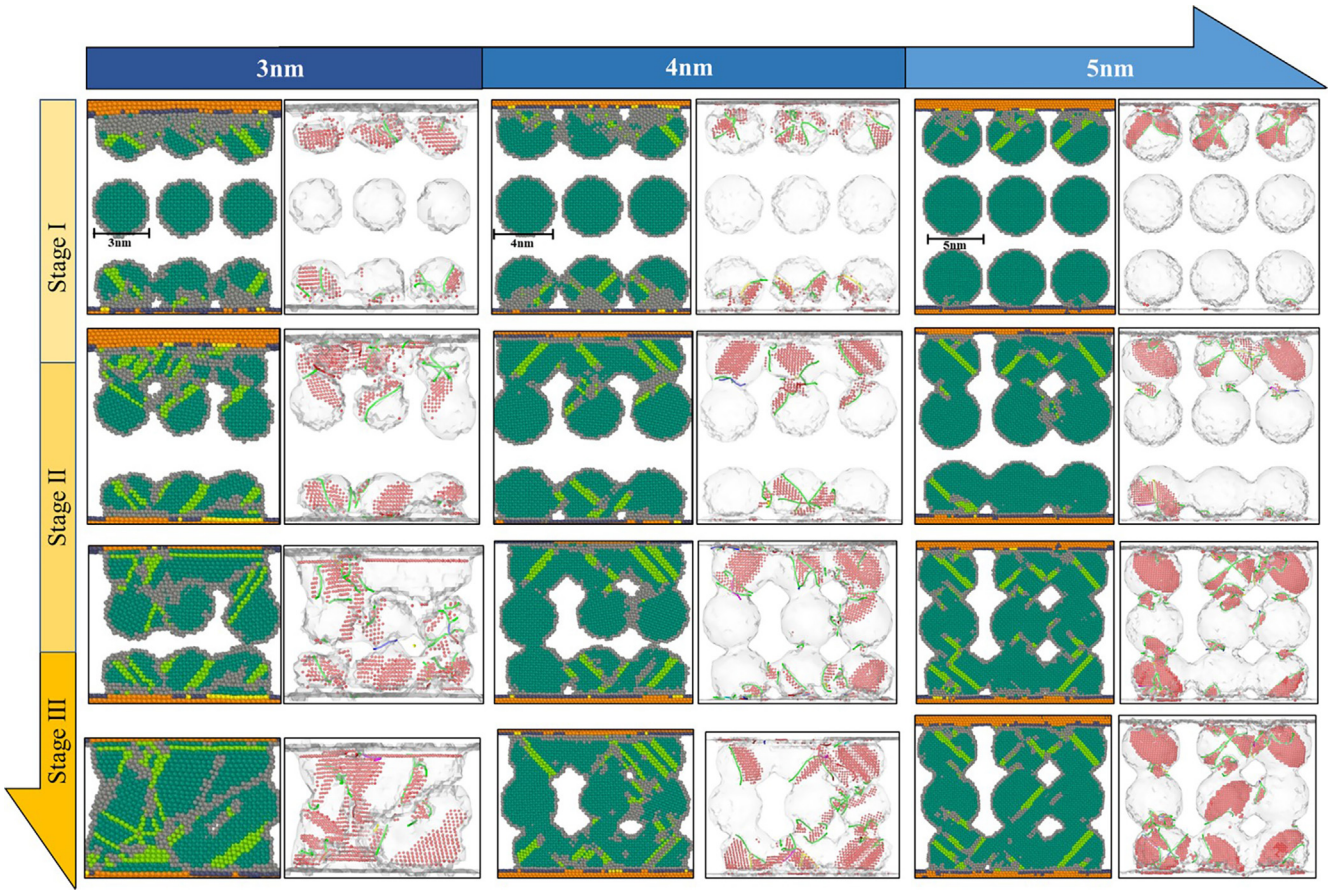

Fig. 9 – Cross-section and dislocation distribution snapshots of different models in different stages. From left to right are models for 3 nm, 4 nm and 5 nm particles. From up to bottom are Stage I, II and III.

curvature. Right after that, NPs are rotated for optimal crystallization positions again through partial dislocation core passing through one of the connected particles [54].

In previous section, we observed the rotation of L1 and L3 particles on the corresponding substrates as well as the secondary rotation of L2 particles caused by L1. First of all, before

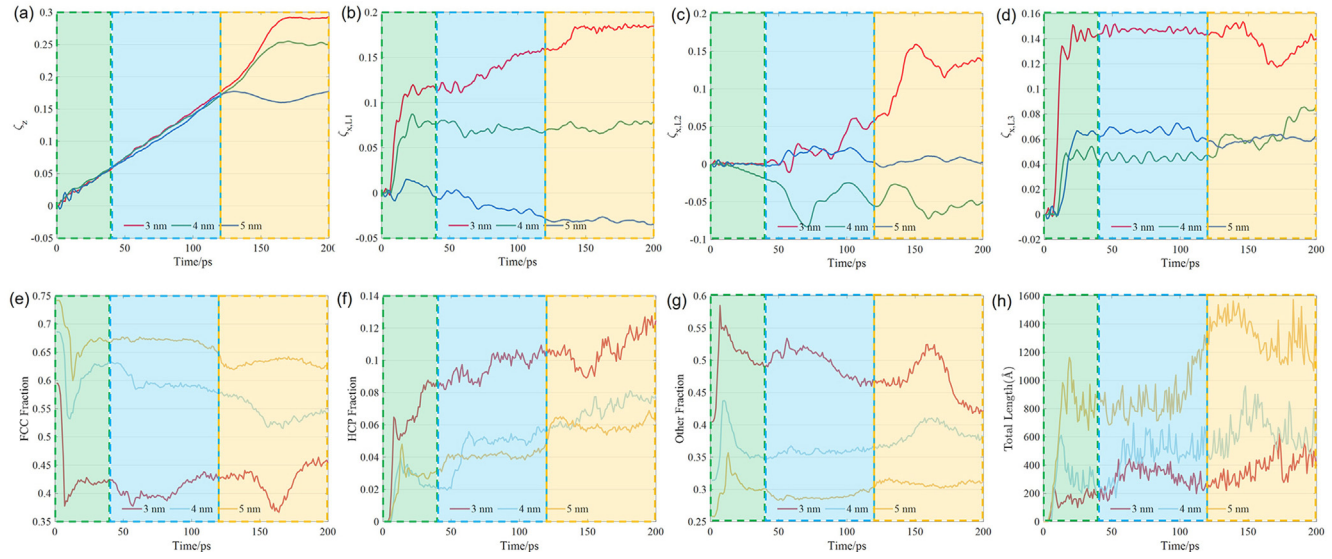

Fig. 10 – Macro- and microstructural evolution during 200 ps sintering for 3 nm, 4 nm and 5 nm models. (a) to (d) The vertical and horizontal shrinkage of L1, L2 and L3. (e) to (g) The diagram of FCC, HCP and amorphous fraction changes over time. (h) The dislocation density.

10 ps, L1 particles began to contact with upper substrate forming the necks. It is clear that atoms of L1 particles at necking region had directional movement towards the type I pores (as shown in Fig. 8a). Similarly, L3 particles had this directional movement as well. L2 did not have any rotation movement yet since the particles were not contacted yet.

Till 60 ps, two different rotation types can be observed within the model: 1) For constraint-free L2 particles, they had the first rotation manner as mentioned above. The misorientation between L2 particles and L1 particles was coming from the rotation of L1 particles in the sintering stage I. Therefore, during the necking formation between L1 particles and L2 particles, the dislocation produced by misorientation would glide across L2 due to the surface stress around the neck groove. It is worth noting that, within each L2 particle, the rotation is not uniformly distributed. More rotation was observed on the part that was near L1 particle. Thus, SF and partial dislocations were produced inside of L2 particles. 2) In L1 and L3, if there were no pinning by substrate, it was supposed to follow the type II rotation manner. As is mentioned in previous studies [55], when there were no misorientation among particles, the particles would contact with their closest neighbor ones and formed crystallization on the interface in short time. Then due to the driving force of annihilation of free surfaces, the crystallized structure at interparticle neck region would rearrange again and transform to amorphous atoms. Right after that, these particles were about to rotate for optimal crystallization positions again through partial dislocation core passing through one of the connected particles. However, due to the pinning effect of substrate to L1 and L3 particles, rigid rotation of particles was impeded. Due to the atomic interaction [56], huge attracting force between neighbored particles still existed, and consequently caused plastic deformation through formation of SF and partial dislocations. Such plastic deformation could finally lead to a partial rotation of each particle, instead of the rotation of the whole particle. By the end of this section, we also compared the size effect of nano particles on rotation. The displacement vector at 60 ps for different size model is shown in Fig. 8(d)–(f). It can be found that, smaller particles had more sever displacement

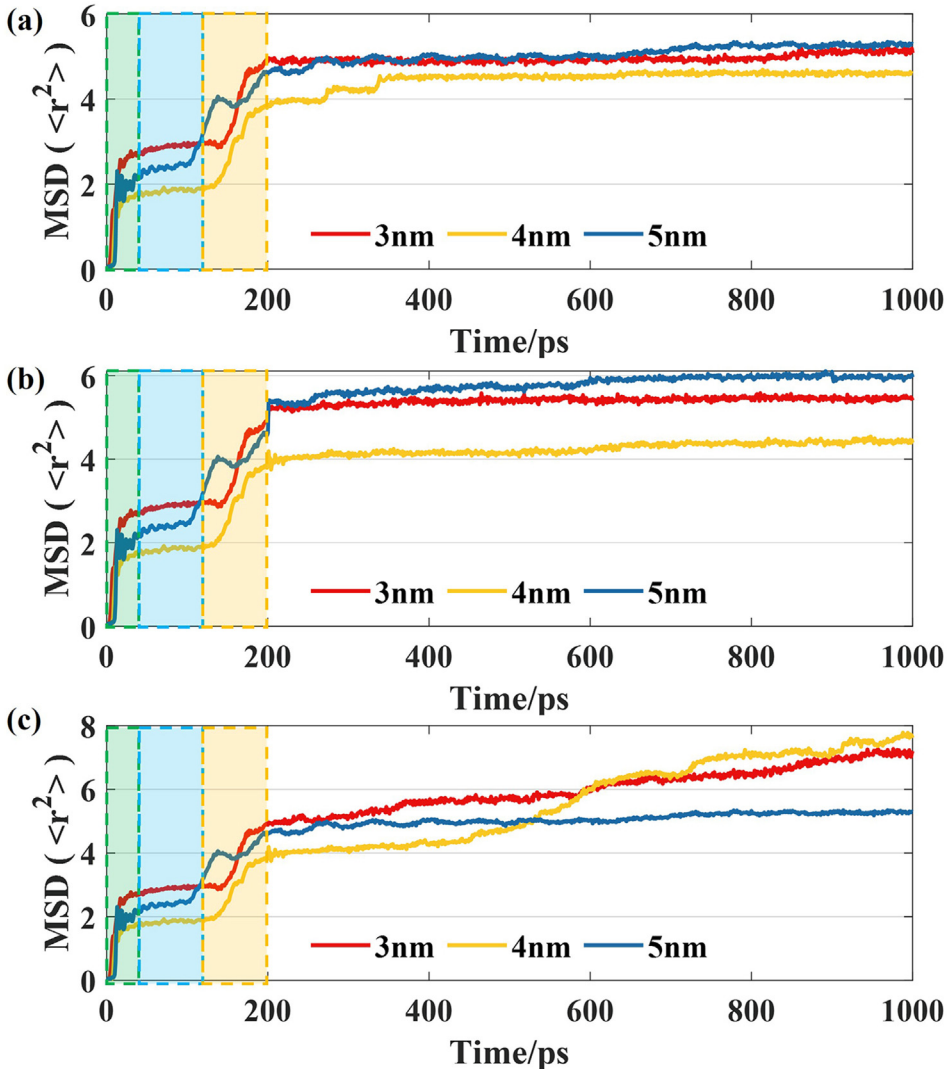

Fig. 11 – Effects of temperature and particle size on the MSD results of copper atoms for 1000 ps. (a) at 500 K. (b) at 600 K. (c) at 700 K.

vector and higher rotation angle as shown in Table 2. It is probably because larger particles model contained smaller surface free energy and thus had less potential for sintering and alignment. However, because of the pinning effect of substrate, rotation angle for each model was reduced, and thus the difference of rotation angle between 4 nm- and 5 nm-model was marginal.

In summary, we found that the particles in this system contained both two rotation manners. Due to the pinning effect of upper and lower substrate, the dislocation mediated alignment process was pronounced. This new proposed rotation phenomenon proved that the annihilation of misorientation could be affected by the substrate.

3.3. *Size effect of NPs-Substrate model on sintering mechanism*

In order to study the size effect on sintering process in our system, 3 nm, 4 nm, 5 nm model were selected. All three models were sintered for 200 ps with same temperature profile. Then the snapshots at critical sintering stage, the shrinkage ratio diagram, the crystal fraction diagram and dislocation density diagram were compared for each model to compare the different microstructural evolution and dislocation behavior. First, for all models, it can be found that the necking on particle-substrate interface was larger than that of particle-particle interface. That is because of the higher free-surface vanishing driving force of substrate surface and wetting between NPs and substrate [43,54]. Second, from Fig. 9 it was found that, smaller-size model closed the pores earlier in each stage. For example, 3 nm model closed all types of pores in 200 ps forming a dense microstructure. However, the 4 nm model and 5 nm model only close type I pores leaving the type II and type III pores. To fully close all pores in these models perhaps requires longer aging time or higher sintering temperature. Furthermore, combining results of DXA, dislocation density curves and crystal fraction curves, it showed that smaller-size model contained more drastic crystal transformation and dislocation evolution in each stage. For instance, in Stage I, L1 and L3 for all three models emerged transformation from FCC to HCP and amorphous. In 3 nm model, more SF across the particles existed indicating more plastic deformation driven neck growth. However, in larger-size model, more stair-rod dislocation appeared in some particles and hindered the plastic deformation. Meanwhile, partial dislocation generated in each model as well. In stage II and III, the 3 nm model again shown better plastic flow ability, and finally, most of dislocations glided into the grain boundaries and annihilated due to the recovery process (as drop shown in dislocation density curve) forming a dense and strong structure. For 4 nm model, the stair-rod dislocation finally unlocked by compressive pressure from the L1 and L2. Most of dislocation glided to the grain boundaries as well. For 5 nm model, dissociating the pinned stair-rod required more plastic deformation and thus needed higher energy input. Therefore, most of stair-rod dislocation stayed at the original location. It is worth noting that the last increasing of dislocation density is attributed to the crystal alignment between L2 and L3 for each model.

Then, from Ez, ExL1 and ExL3 curve (Fig. 10) it was shown that smaller-size models usually contained higher shrinkage ratio which is in line with previous studies [22,54,55]. Specifically, L1 layer of 3 nm model had around 18% shrinkage ratio which is way higher than that for 4 nm model (9%) and 5 nm model (−5%). Interestingly, there were negative shrinkage values in L1 of 5 nm and L2 of 4 nm. For 4 nm model, the reason (rigid rotation and randomly elastic oscillation of L1) has been discussed in the previous sections. For 5 nm model scenario, the expansion of L2 started in stage II when the L1 contacted with it. This phenomenon confirmed the size effect on larger pores formation. For L3, there is no influence of pressure at the first two stages, and therefore, could be used to study the size effect on particle-substrate sintering behavior. It can be found that, smaller-size model reached the stable state on substrate earlier than the larger-size one. Furthermore, in the context of atomic simulations, the sintering mechanisms are temperature-dependent. This arises because by enhancing the temperature, surface diffusion, volume diffusion beneath the surface, grain boundary diffusion, and even evaporation and recondensation will be activated. Accordingly, to more accurately explore the effect of sintering temperature on the sintering mechanisms, in addition to the studied 500 K sintering, the prescribed models were sintered at 600 K and 700 K. Then these as-sintered models were kept at each peak temperature till 1000 ps. As is shown in Fig. 11 the MSD results for 500 K and 600 K were plateau in the aging stage. That is to say, the atomic diffusion was not significantly activated at this low temperature. Meanwhile at high temperature (700 K) the atomic diffusion was dominant after 200 ps. It was deduced that the atomic diffusion was driven by the closure of pores. Since smaller pores contained larger surface curvature, they could provide higher driving force. It was found that the 3 nm and 4 nm had better motion. Whereas for 5 nm particles, after type-I pore was closed, the rest of large type-II and type-III were too big to drive the diffusion motion.

4. Conclusion

A molecular dynamic (MD) simulation was carried out to study the coalescence kinetics and microstructure evolution of Cu nanoparticles sintering on substrates at low temperature. A sandwich-structure model containing two substrate and multiple particles in between was used in this study. It is found that at low temperature the dominating sintering mechanism is plastic flow caused by dislocation production and motion. The pressure provided by the upper substrate can significantly accelerating the sintering behavior by amplifying the plastic flow. Furthermore, the rigid rotation was observed during the coalescence process, and it may cause random misorientation and elastic oscillation of particles. Moreover, the pinning effect of substrate on particles may expand such random motion of particles in L2, which may produce huge pores. These pores can be vanished via both plastic deformation and surface diffusion. For all models, it can be found that the necking on particle-substrate interface was larger than that of particle-particle interface. Secondly, we found that the particles in this system contained both two rotation

manners. Due to the pinning effect of upper and lower substrate, the dislocation mediated alignment process was pronounced. This new proposed rotation phenomenon proved that the annihilation of misorientation could be affected by the substrate. Finally, to study the size and temperature effect on sintering process in our system, 3 nm, 4 nm, 5 nm model were selected and aged at 500 K, 600 K and 700 K for longer time. It was found that smaller-size models usually contained higher shrinkage ratio and smaller pores. Also, smaller-size model contained more drastic crystal transformation and dislocation evolution in each stage.

Declaration of Competing Interest

The authors declare that they have no known competing financial interests or personal relationships that could have appeared to influence the work reported in this paper.

Acknowledgement

This work was supported by the National Key R&D Program of China (2018YFE0204600) and the Shenzhen Fundamental Research Program (JCYJ20200109140822796).

Appendix A. Supplementary data

Supplementary data to this article can be found online at https://doi.org/10.1016/j.jmrt.2022.01.052.

REFERENCES

[1] Chen C, Suganuma K. Microstructure and mechanical properties of sintered Ag particles with flake and spherical shape from nano to micro size. Mater Des 2019;162:311–21. https://doi.org/10.1016/j.matdes.2018.11.062.
[2] Noh S, Choe C, Chen C, Suganuma K. Heat-resistant die-attach with cold-rolled Ag sheet. APEX 2018;11:016501. https://doi.org/10.7567/APEX.11.016501.
[3] Suganuma K, Nagao S, Sugahara T, Yokoi E, Zhang H, Jiu J. Silver sinter joining and stress migration bonding for WBG die-attach. In: 2016 int. Symp. 3D power electron. Integr. Manuf. 3D-PEIM; 2016. p. 1–17. https://doi.org/10.1109/3DPEIM.2016.7570554.
[4] Liu X, He S, Nishikawa H. Thermally stable Cu3Sn/Cu composite joint for high-temperature power device. Scripta Mater 2016;110:101–4. https://doi.org/10.1016/j.scriptamat.2015.08.011.
[5] Li D, Mei Y, Xin Y, Li Z, Chu PK, Ma C, et al. Reducing migration of sintered Ag for power devices operating at high temperature. IEEE Trans Power Electron 2020;35:12646–50. https://doi.org/10.1109/TPEL.2020.2994343.
[6] Lu G-Q, Mei Y, Wang M, Li X. Low-temperature silver sintering for bonding 3D power modules. In: 2019 6th int. Workshop low temp. Bond. 3D integr. LTB-3D; 2019. https://doi.org/10.23919/LTB-3D.2019.8735123. 19–19.
[7] Xie Y, Wang Y, Mei Y, Xie H, Zhang K, Feng S, et al. Rapid sintering of nano-Ag paste at low current to bond large area (>100 mm2) power chips for electronics packaging. J Mater Process Technol 2018;255:644–9. https://doi.org/10.1016/j.jmatprotec.2018.01.017.
[8] Yan H, Mei Y-H, Wang M, Li X, Lu G-Q. Pressureless sintering multi-scale Ag paste by a commercial vacuum reflowing furnace for massive production of power modules. J Mater Sci Mater Electron 2019;30:9634–41. https://doi.org/10.1007/s10854-019-01297-x.
[9] Quintero PO, McCluskey FP. Temperature cycling reliability of high-temperature lead-free die-attach technologies. IEEE Trans Device Mater Reliab 2011;11:531–9. https://doi.org/10.1109/TDMR.2011.2140114.
[10] George E, Pecht M. Process occurs through atomic transportation (mass transportation) at the contact area of particles. Microelectron Reliab 2016;65:1–7. https://doi.org/10.1016/j.microrel.2016.07.150.
[11] George E, Das D, Osterman M, Pecht M. Thermal cycling reliability of lead-free solders (SAC305 and Sn3.5Ag) for high-temperature applications. IEEE Trans Device Mater Reliab 2011;11:328–38. https://doi.org/10.1109/TDMR.2011.2134100.
[12] Gao Y, Chen C, Nagao S, Suganuma K, Bahman AS, Iannuzzo F. Highly reliable package using Cu particles sinter paste for next generation power devices. In: PCIM eur. 2019 int. Exhib. Conf. Power electron. Intell. Motion renew. Energy energy manag.; 2019. p. 1–4.
[13] Yuan Y, Wu H, Li J, Zhu P, Sun R. Cu-Cu joint formation by low-temperature sintering of self-reducible Cu nanoparticle paste under ambient condition. Appl Surf Sci 2021;570:151220. https://doi.org/10.1016/j.apsusc.2021.151220.
[14] Zhang B, Damian A, Zijl J, van Zeijl H, Zhang Y, Fan J, et al. In-air sintering of copper nanoparticle paste with pressure-assistance for die attachment in high power electronics. J Mater Sci Mater Electron 2021;32:4544–55. https://doi.org/10.1007/s10854-020-05196-4.
[15] Zhang Y, Zhu P, Li G, Chen L, Cui C, Zhang K, et al. Easy separation of CuO nanocrystals with high catalytic activity. Mater Lett 2018;212:332–5. https://doi.org/10.1016/j.matlet.2017.10.127.
[16] Chen C, Iwaki A, Suetake A, Sugiura K, Kanie K, Suganuma K. Low temperature Cu sinter joining on different metallization substrates and its reliability evaluation with a high current density. In: 2021 33rd int. Symp. Power semicond. Devices ICs ISPSD; 2021. p. 387–90. https://doi.org/10.23919/ISPSD50666.2021.9452283.
[17] Gao Y, Li W, Chen C, Zhang H, Jiu J, Li C-F, et al. Novel copper particle paste with self-reduction and self-protection characteristics for die attachment of power semiconductor under a nitrogen atmosphere. Mater Des 2018;160:1265–72. https://doi.org/10.1016/j.matdes.2018.11.003.
[18] Gao Y, Takata S, Chen C, Nagao S, Suganuma K, Bahman AS, et al. Reliability analysis of sintered Cu joints for SiC power devices under thermal shock condition. Microelectron Reliab 2019;100–101:113456. https://doi.org/10.1016/j.microrel.2019.113456.
[19] Kang S-JL. Sintering: densification, grain growth, and microstructure. Amsterdam: Elsevier; 2005.
[20] Paul S, Nagahanumaiah, Mitra S, Roy D. Molecular dynamics simulation study of neck growth in micro-selective laser sintering of copper nanoparticles. In: Dixit US, Kant R, editors. Simul. Des. Manuf. Singapore: Springer Singapore; 2018. p. 259–92. http://link.springer.com/10.1007/978-981-10-8518-5_10. [Accessed 6 June 2020].
[21] Wang J. Mass transport of metallic nanostructures during sintering process: a molecular dynamics perspective. 2019.
[22] Cheng B, Ngan AHW. The sintering and densification behaviour of many copper nanoparticles: a molecular dynamics study. Comput Mater Sci 2013;74:1–11. https://doi.org/10.1016/j.commatsci.2013.03.014.
[23] Guo JY, Xu CX, Hu AM, Oakes KD, Sheng FY, Shi ZL, et al. Sintering dynamics and thermal stability of novel configurations of Ag clusters. J Phys Chem Solid 2012;73:1350–7. https://doi.org/10.1016/j.jpcs.2012.06.010.

[24] Hu D, Cui Z, Fan J, Fan X, Zhang G. Thermal kinetic and mechanical behaviors of pressure-assisted Cu nanoparticles sintering: a molecular dynamics study. Results Phys 2020;19:103486. https://doi.org/10.1016/j.rinp.2020.103486.
[25] Yang L, Gan Y, Zhang Y, Chen JK. Molecular dynamics simulation of neck growth in laser sintering of different-sized gold nanoparticles under different heating rates. Appl Phys A 2012;106:725–35. https://doi.org/10.1007/s00339-011-6680-x.
[26] Wakai F, Guillon O, Okuma G, Nishiyama N. Sintering forces acting among particles during sintering by grain-boundary/surface diffusion. J Am Ceram Soc 2018;102(2):538–47. https://doi.org/10.1111/jace.15716.
[27] Li C, Li D, Tao X, Chen H, Ouyang Y. Molecular dynamics simulation of diffusion bonding of Al–Cu interface. Model Simulat Mater Sci Eng 2014;22:065013. https://doi.org/10.1088/0965-0393/22/6/065013.
[28] Cheng B, Ngan AHW. Crystal plasticity of Cu nanocrystals during collision. Mater Sci Eng 2013;585:326–34. https://doi.org/10.1016/j.msea.2013.07.065.
[29] Dong H, Moon K-S, Wong CP. Molecular dynamics study on the coalescence of Cu nanoparticles and their deposition on the Cu substrate. J Electron Mater 2004;33:1326–30. https://doi.org/10.1007/s11664-004-0161-3.
[30] koraychy EE, Meddad M, Badawi M, Mazroui M. Sintering and deposition of homo- and heteronanoparticles of aluminum and nickel on aluminum (100) substrate. Chem Phys 2021;541:111037. https://doi.org/10.1016/j.chemphys.2020.111037.
[31] Zhan L, Zhu X, Qin X, Wu M, Li X. Sintering mechanism of copper nanoparticle sphere-plate of crystal misalignment: a study by molecular dynamics simulations. J Mater Res Technol 2021;12:668–78. https://doi.org/10.1016/j.jmrt.2021.03.029.
[32] Wang J, Shin S, Hu A, Wilt JK. Diffusion kinetics of transient liquid phase bonding of Ni-based superalloy with Ni nanoparticles: a molecular dynamics perspective. Comput Mater Sci 2018;152:228–35. https://doi.org/10.1016/j.commatsci.2018.05.056.
[33] Ishikawa D, An BN, Mail M, Wurst H, Leyrer B, Blank T, et al. Bonding strength of Cu sinter die-bonding paste on Ni, Cu, Ag, and Au surfaces under pressureless bonding process. Trans Jpn Inst Electron Packag 2020;13:199-017-1–E19-017–11. https://doi.org/10.5104/jiepeng.13.E19-017-1.
[34] Plimpton S. Fast parallel algorithms for short- range molecular dynamics. Model Simulat Mater Sci Eng 2009;18:44. https://doi.org/10.1006/jcph.1995.1039.
[35] Daw MS, Baskes MI. Embedded-atom method: derivation and application to impurities, surfaces, and other defects in metals. Phys Rev B 1984;29:6443–53. https://doi.org/10.1103/PhysRevB.29.6443.
[36] Fischer F, Schmitz G, Eich SM. A systematic study of grain boundary segregation and grain boundary formation energy using a new copper–nickel embedded-atom potential. Acta Mater 2019;176:220–31. https://doi.org/10.1016/j.actamat.2019.06.027.
[37] Liu Z. Sintering neck growth mechanism of Fe nanoparticles: a molecular dynamics simulation. Chem Eng Sci 2020;218(8):115583. https://doi.org/10.1016/j.ces.2020.115583.
[38] Malti A, Kardani A, Montazeri A. An insight into the temperature-dependent sintering mechanisms of metal nanoparticles through MD-based microstructural analysis. Powder Technol 2021;386:30–9. https://doi.org/10.1016/j.powtec.2021.03.037.
[39] Li S, Liu Y, Sun F, Fang H. Multi-particle molecular dynamics simulation: shell thickness effects on sintering process of Cu-Ag core-shell nanoparticles. J Nanoparticle Res 2021;23:6. https://doi.org/10.1007/s11051-021-05144-1.
[40] Wang J, Shin S. Sintering of multiple Cu-Ag core-shell nanoparticles and properties of nanoparticle-sintered structures. RSC Adv 2017;7:21607–17. https://doi.org/10.1039/c7ra02611k.
[41] Yang S, Kim W, Cho M. Molecular dynamics study on the coalescence kinetics and mechanical behavior of nanoporous structure formed by thermal sintering of Cu nanoparticles. Int J Eng Sci 2018;123:1–19. https://doi.org/10.1016/j.ijengsci.2017.11.008.
[42] Li S, Liu Y, Ye H, Liu X, Sun F, Fan X, et al. Sintering mechanism of Ag nanoparticle-nanoflake: a molecular dynamics simulation. J Mater Res Technol 2022;16:640–55. https://doi.org/10.1016/j.jmrt.2021.12.029.
[43] Samsonov VM, Bembel AG, Popov IV, Vasilyev SA, Talyzin IV. Solid-state wetting at the nanoscale: molecular dynamics and surface diffusion approach. Surf Innov 2017;5:9.
[44] Ren X, Li X, Huang C, Yin H, Wei F. Molecular dynamics simulation of thermal welding morphology of Ag/Au/Cu nanoparticles distributed on Si substrates. Ferroelectrics 2020;564:19–27. https://doi.org/10.1080/00150193.2020.1761698.
[45] Wang F, Tang Z, He H. Stress-dislocation interaction mechanism in low-temperature thermo-compression sintering of Ag NPs. AIP Adv 2018;8(4):045012. https://doi.org/10.1063/1.5024593.
[46] Samantaray M. Computational modeling of heat transfer and sintering behavior during direct metal laser sintering of AlSi10Mg alloy powder. C R Mec 2018;346(11):1043–54. https://doi.org/10.1016/j.crme.2018.08.006.
[47] Stukowski A. Structure identification methods for atomistic simulations of crystalline materials. Model Simulat Mater Sci Eng 2012;20. https://doi.org/10.1088/0965-0393/20/4/045021.
[48] Stukowski A, Bulatov VV, Arsenlis A. Automated identification and indexing of dislocations in crystal interfaces. Model Simulat Mater Sci Eng 2012;20:085007. https://doi.org/10.1088/0965-0393/20/8/085007.
[49] Huang Y-R, Chuang P-H, Chen C-L. Molecular-dynamics calculation of the thermal conduction in phase change materials of graphene paraffin nanocomposites. Int J Heat Mass Tran 2015;91:45–51. https://doi.org/10.1016/j.ijheatmasstransfer.2015.07.110.
[50] Mehrer H. Diffusion in solids: fundamentals, methods, materials, diffusion-controlled processes. Springer Science & Business Media; 2007.
[51] Cheng B, Ngan AHW. The crystal structures of sintered copper nanoparticles: a molecular dynamics study. Int J Plast 2013;47:65–79. https://doi.org/10.1016/j.ijplas.2013.01.006.
[52] Lange AP, Samanta A, Majidi H, Mahajan S, Ging J, Olson TY, et al. Dislocation mediated alignment during metal nanoparticle coalescence. Acta Mater 2016;120:364–78. https://doi.org/10.1016/j.actamat.2016.08.061.
[53] Nelli D, Rossi G, Wang Z, Palmer RE, Ferrando R. Structure and orientation effects in the coalescence of Au clusters. Nanoscale 2020;12:7688–99. https://doi.org/10.1039/C9NR10163B.
[54] Wang J, Shin S, Hu A. Geometrical effects on sintering dynamics of Cu-Ag core-shell nanoparticles. J Phys Chem C 2016;120:17791–800. https://doi.org/10.1021/acs.jpcc.6b05515.
[55] Song P, Wen D. Molecular dynamics simulation of the sintering of metallic nanoparticles. J Nanoparticle Res 2010;12:823–9. https://doi.org/10.1007/s11051-009-9718-7.
[56] Wang J, Chen S, Cui K, Li D, Chen D. Approach and coalescence of gold nanoparticles driven by surface thermodynamic fluctuations and atomic interaction forces. ACS Nano 2016;10:2893–902. https://doi.org/10.1021/acsnano.5b08236.